

# ***In situ* visualizing the recognition between proteins and platinum-damaged DNA in single cells by correlated optical and secondary ion mass spectrometric imaging**

Yu Lin<sup>1,2,3,11</sup>, Kui Wu<sup>1,2,3,5,11</sup>, Feifei Jia<sup>1,2,3,4,11</sup>, Ling Chen<sup>1,2,3</sup>, Zhaoying Wang<sup>1,2,3</sup>, Yanyan Zhang<sup>1,2,3</sup>, Qun Luo<sup>1,2,3,6</sup>, Suyan Liu<sup>1,2,3</sup>, Luyu Qi<sup>1,2,3,6</sup>, Nan Li<sup>2,3,6,7</sup>, Xiaohong Fang<sup>2,3,6,7</sup>, Pu Dong<sup>8</sup>, Fei Gao<sup>9</sup>, Yao Zhao<sup>1,2,3\*</sup>, Fuyi Wang<sup>1,2,3,4,6,10\*</sup>

<sup>1</sup> CAS Key Laboratory of Analytical Chemistry for Living Biosystems, Institute of Chemistry, Chinese Academy of Sciences, Beijing, 100190, People's Republic of China;

<sup>2</sup>Beijing National Laboratory for Molecular Sciences;

<sup>3</sup> CAS Research/Education Center for Excellence in Molecular Sciences;

<sup>4</sup> National Centre for Mass Spectrometry in Beijing;

<sup>5</sup> Key Laboratory of Hubei Province for Coal Conversion and New Carbon Materials; School of Chemistry and Chemical Engineering, Wuhan University of Science and Technology, Wuhan, 430081, People's Republic of China;

<sup>6</sup> University of Chinese Academy of Sciences, Beijing 100049, People's Republic of China;

<sup>7</sup> CAS Key Laboratory of Molecular Nanostructure & Nanotechnology, Institute of Chemistry, Chinese Academy of Sciences, Beijing, 100190, People's Republic of China;

<sup>8</sup> Institute of Information Engineering, Chinese Academy of Sciences, Beijing, 100093, People's Republic of China;

<sup>9</sup> China Telecom Corporation Limited Beijing Research Institute, Beijing, 100035, People's Republic of China;

<sup>10</sup> Basic Medical College, Shandong University of Chinese Traditional Medicine, Jinan 250355, P. R. China;

<sup>11</sup> These authors contributed equally: Yu Lin, Kui Wu, Feifei Jia.

\*Email: fuyi.wang@iccas.ac.cn, yaozhao@iccas.ac.cn

***In situ* visualization of the recognition and interaction between proteins and drug damaged DNA at single cell level is highly important for understanding the molecular mechanism of action of DNA targeting drugs, yet a great challenge. We herein report a novel approach, termed as correlated optical and secondary ion mass spectrometric imaging (COSIMSi), for exploring the recognition between proteins and cisplatin-damaged DNA in single cells. Genetically encoded EYFP-fused HMGB1, an *in vitro* well-known specific binder of cisplatin-damaged DNA, and dye-stained DNA, and cisplatin were mapped by LSCM and ToF-SIMS imaging, respectively. The LSCM and SIMS images were aligned with aiding of an addressable silicon wafer to generate fused images, in which the co-localization of the fluorescence and MS signals indicated the formation of HMGB1-Pt-DNA ternary complexes in a dose- and time-dependent manner. In contrast, COSIMSi**

showed that little HMGB1(F37A)-Pt-DNA complex was produced under the same conditions. Moreover, we demonstrated for the first time that cisplatin lesion on DNA prevented a DNA-binding protein Smad3 from interacting with DNA. These results verify that the COSIMSi is an effective and straightforward tool for *in situ* visualization of recognition and interaction between proteins and specific damaged DNA in single cells.

### Abbreviations

Ab: antibody

AFM: atomic force microscopy

COSIMSi: correlated optical and secondary ion mass spectrometry imaging

EGFP: enhanced green fluorescent protein

EYFP: enhanced yellow fluorescent protein

FISH: fluorescence in situ hybridization

HMGB1: high mobility group box 1 protein

LSCM: laser scanning confocal microscope

PBS: phosphate-buffered saline

PC4: nuclear protein positive cofactor

STED: stimulated emission depletion

ToF-SIMS: time of flight secondary ion mass spectrometry

### Introduction

DNA damage is of great concern in the research of gene mutation, and in the molecular mechanism of action of DNA targeting anticancer drugs such as cisplatin and doxorubicin. Cisplatin, a greatly successful anticancer drug in clinic, has been extensively explored for its mechanism of action. Although the interactions with proteins and other sulfur-containing cellular components may be implicated to some extent in mechanism of action of cisplatin<sup>1</sup>, and mitochondria DNA is also an important target of cisplatin<sup>2</sup>, it is widely accepted that cisplatin exert its anticancer activity by binding to nuclear DNA<sup>3</sup>. Cisplatin forms mainly 1,2-intrastrand cross-linked adducts on -GpG- or -ApG- sites of DNA and thus induces a series of variation on the conformation of DNA such as bending and unwinding of the duplex<sup>4,5</sup>. A variety of DNA damage recognition and repair proteins, such as nucleotide excision repair proteins<sup>6</sup> and mismatch repair proteins<sup>7</sup> have been demonstrated previously to bind specifically to cisplatin damaged DNA. Among them, high mobility group box 1 (HMGB1), an abundant and highly conserved nucleoprotein<sup>8</sup>, selectively binds to 1,2-intrastrand cisplatin-crosslinked DNA. The high-resolution crystal structure of a cisplatin-crosslinked DNA-HMGB1a complex, where HMGB1a refers to the A domain of HMGB1, has been reported in 1999.<sup>9</sup> Thereafter the recognition and interaction between HMGB1 and cisplatin-damaged DNA as well as their biological implications have been extensively studied in cell-free media including recombinant chromosomes<sup>3,4,10</sup>. Given the complex cellular micro-environment around the cisplatin damaged DNA, the researches conducted in cell-free media may not fully represent the recognition and interaction between HMGB1 and cisplatin-crosslinked DNA inside

cells. To address this issue, in this work, we aim at *in situ* visualizing and verifying the recognition and interaction of specific proteins, in particular, HMGB1 with cisplatin damaged DNA in single cells by developing a novel strategy by combining laser scanning confocal fluorescence microscopy (LSCM) and time of flight secondary ion mass spectrometry (ToF-SIMS) imaging, which we termed as correlated optical and SIMS imaging (COSIMSi).

SIMS, including NanoSIMS and ToF-SIMS, is a powerful surface analysis technique in the field of elemental, isotopic, and molecular analysis. In recent years, the application of SIMS has been extended from the analysis of solid material samples such as semiconductors and planetary dusts to biological samples, e.g. botanic, paleontological, microbiologic and biomedical samples<sup>11,12</sup>. However, directly *in situ* imaging of biological macromolecules such as proteins and DNAs in single-cells is still a great challenge due to weak and even absent signals of the corresponding molecular ions or informative fragment ions<sup>13-15</sup>. To address this issue, stable isotopic labeling to proteins and DNA has been proved to be a good option<sup>16,17</sup>. Genetically encoded proteins tagged with chemical labels by bio-orthogonal reactions could also be applied<sup>18,19</sup>. Alternatively, LSCM and stimulated emission depletion (STED) nanoscopy imaging in combination with genetic<sup>18,20</sup> or fluorescence *in situ* hybrid (FISH) labeling<sup>21</sup> were utilized to localize biomacromolecules and organelles. Effective correlated imaging using NanoSIMS for chemicals and LSCM/STED for cell morphology can integrate both of their advantages, so as to determine the subcellular distribution of target molecules and more importantly, build a connection between two different indicators at single cell level.<sup>16-19,21,22</sup>

In this work, we tagged HMGB1 with enhanced yellow fluorescent protein (EYFP) in HeLa cells so that the fluorescence of EYFP indicates the location of HMGB1 inside cells. Then the cells were incubated with the platinum based anticancer drug, cisplatin. The Pt-bound DNA was mapped by ToF-SIMS for Pt in combined with the confocal fluorescence imaging for nucleus DNA. Finally, we used a software ImageJ<sup>®</sup> to precisely align the position and angle of the images from SIMS and LSCM imaging. The superposition of EYFP fused HMGB1 and Pt-bound DNA evidenced the recognition between HMGB1 and Pt-damaged DNA, and the formation of HMGB1-cisplatin-DNA ternary complexes inside cells. Our studies demonstrated that integration of ToF-SIMS imaging for Pt drugs and LSCM imaging for their biological targets inside cells provides valuable information for better understanding in the mechanism of action of drugs.

## Results

### Mapping cellular distribution of cisplatin by ToF-SIMS

Before performing ToF-SIMS imaging on cells, we first employed argon gas cluster ion beam (GCIB) to sputter the cell surface to remove any contaminants as well as membrane components. As shown in Fig. 1a,b,g and Supplementary Fig. 1, the lyophilized HeLa cells on silicon wafer were decreased in sizes after sputtered by GCIB for a few cycles. Usually 5 – 15 cycles of GCIB sputtering was performed until the

signal of total ions obtained by 5 analytical scans using  $\text{Bi}_3^+$  ion beam could clearly render the cell morphology (Fig. 1e and Supplementary Fig. 1), which indicates that the contaminants and membrane components have been removed. In contrast, the analytical scans using  $\text{Bi}_3^+$  ion beam, even up to 1000 – 3000 times, did not make significant change on the morphology of the lyophilized cells (Fig. 1a,b,g,l and Supplementary Fig. 2). These imply that the removal of cell membrane and top cytoplasm layer by GCIB sputtering will not impact the ToF-SIMS imaging of nuclei, where the interaction of cisplatin-damaged DNA with proteins takes place.

NanoSIMS has been previously applied to map the subcellular distribution of cisplatin, showing in combination with LSCM imaging that cisplatin located in both cytoplasm, in particular lysosomes, and nuclei<sup>23</sup>. Herein, we use for the first time ToF-SIMS to visualize cisplatin inside cells. The mass spectrum (Supplementary Fig. 3) shows that cisplatin was detected as a recombinant fragment,  $[\text{PtCN}]^-$ , which appears to be the characteristic fragment arising from platinum complexes during ToF-SIMS analysis<sup>24</sup>. The presence of three major isotopes,  $^{194}\text{Pt}$ ,  $^{195}\text{Pt}$  and  $^{196}\text{Pt}$ , of platinum conferred the ion peak of  $[\text{PtCN}]^-$  with distinguished isotopic pattern (Supplementary Fig. 3), allowing precisely localization of cisplatin inside cells by ToF-SIMS *via* the characterized isotopic ions at  $m/z$  220, 221 and 222 (Supplementary Fig. 4). It is worth pointing out that the ToF-SIMS image did not show localization of cisplatin in the cytoplasm region<sup>23</sup> as GCIB sputtering might have removed most of cytoplasm layer before SIMS imaging (Fig. 1 and Supplementary Fig. 1 – 2). However, the removal of the cytoplasm did not impact the SIMS imaging on the nucleus area as evidenced by the full and clear outline of the nucleus rendered by  $[\text{PtCN}]^-$  ions (Supplementary Fig. 4).

### Development and validation of COSIMSi method

As mentioned earlier, neither NanoSIMS nor ToF-SIMS can directly map native proteins inside cells due to lack of informative ions. Therefore, we alternatively applied LSCM to visualize HMGB1 protein inside the cells in the present work. To do so, we constructed the enhanced yellow fluorescent protein (EYFP) fused HMGB1 plasmid by inserting the HMGB1 coding sequence into the multiple clone site (MCS) of pEYFP-N1 vector (Supplementary Fig. 5), and then transfected the fused plasmid into HeLa cells. Both Western blotting assays (Supplementary Fig. 6) and LSCM imaging (Fig. 1d) indicate the successful expression of the EYFP-HMGB1 fusion protein in HeLa cells, where the fused protein was shown to locate at cytoplasm and nucleus which was stained by the non-specific DNA fluorescence dye DAPI (Fig. 1c).

Next, we performed ToF-SIMS imaging on the EYFP-HMGB1 overexpressed HeLa cells. It is a challenge to locate a micrometer region of interest in a silicon wafer for successive optical and SIMS imaging. Wessles and co-workers achieved this by using the multiphoton laser beam at maximum energy to create a few location markers on the cell sample *via* deforming the LR white resin which was used to embed cells<sup>20</sup>. Here, as reported previously<sup>25</sup>, we cultured cells on a patterned silicon wafer with  $200 \times 200 \mu\text{m}$  squares (Fig. 1b,g,l) such that we can easily locate one or a few specific cells for successive LSCM and ToF-SIMS imaging. Following the LSCM images on a

lyophilized cell framed in the red box (Fig. 1c,d), we scanned the cell surface using  $\text{Bi}_3^+$  ion beam for 10 times to gain the image of the cell indicated by total ions signal (Fig. 1e). Then, aided by the addressable silicon wafer we used ImageJ<sup>®</sup> software to precisely align the position and angle of the images obtained by LSCM and SIMS imaging to produce fused images of LSCM and SIMS imaging. As shown in Fig. 1f, the nuclear morphology of the cell rendered by SIMS image of the total ions well matched those visualized by LSCM images of EYFP-HMGB1 and DAPI. Furthermore, we recorded SIMS images of the cell which was sputtered 5 cycles by GCIB, and then fused the LSCM images with the SIMS images of total ions,  $\text{Cl}^-$  and  $\text{PO}_3^-$  (Fig. 1h – j), the later ion arisen from endogenous biomolecules such as phospholipids, phosphoproteins and RNA/DNA. The images of  $\text{Cl}^-$  and  $\text{PO}_3^-$  ions well outlined the cell membrane and nucleus, respectively. Moreover, the SIMS image of total ions and its overlap with the fluorescent images (Fig. 1k) shows that 5 cycles of GCIB sputtering effectively remove all contaminants and membrane components on the cell surface. When we further scanned the residual cell using  $\text{Bi}_3^+$  ion beam for 3000 times to map the distribution of  $\text{Cl}^-$  and  $\text{PO}_3^-$  ions, the signals of both ions significantly increased with increase in scan times, well rendering the morphology of the nucleus (Fig. 1m – p).

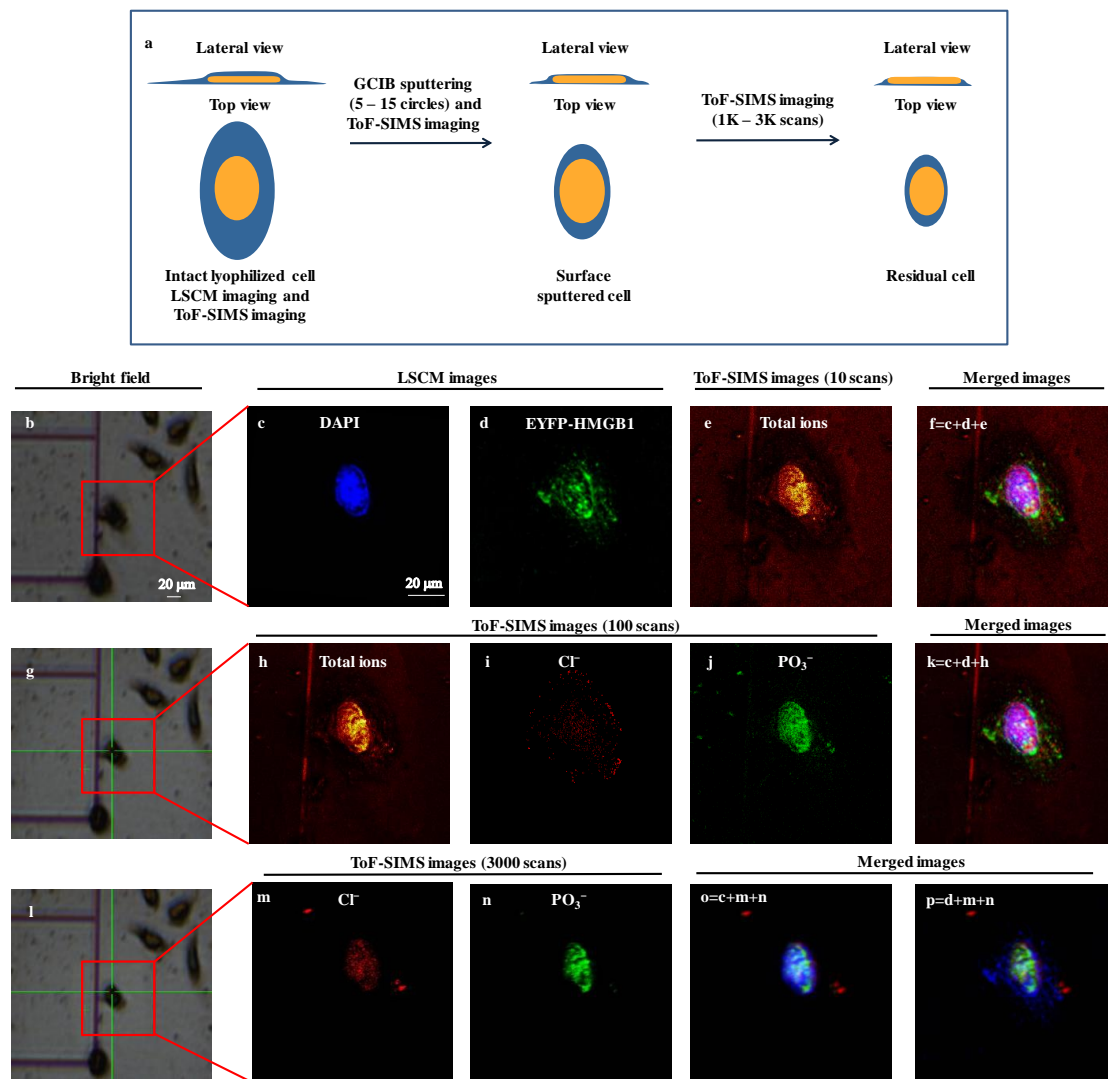


**Fig. 1 | COSIMS imaging of single cells.** **a**, Workflow of the COSIMS imaging of a single cell. **b – f**, COSIMS imaging of a intact lyophilized cell: **(b)** bright field image, **(c, d)** LSCM imaging of DAPI stained nucleus **(c)** and EYFP-HMGB1 **(d)**, **(e)** ToF-SIMS image of total ions (10 scans of ToF-SIMS imaging using  $\text{Bi}_3^+$  ion beam), and **(f)** merged image of LSCM images of DAPI (blue), EYFP-HMGB1 (green) and ToF-SIMS image of total ions (red); **g – k**, COSIMS imaging of the lyophilized cell which was sputtered by 5 cycles using GCIB after LSCM imaging, followed by 100 scans of ToF-SIMS imaging using  $\text{Bi}_3^+$  ion beam: **(g)** bright field images, **(h – j)** ToF-SIMS images of total ions **(h)**,  $\text{Cl}^-$  **(i)** and  $\text{PO}_3^-$  **(j)** of the single cell, **(k)** merged image of ToF-SIMS image **(h)** and LSCM images (HMGB1: green and DAPI: blue); **l – p**, COSIMS imaging of the lyophilized cell which was sputtered by 5 cycles using GCIB, followed by 3000 scans of ToF-SIMS imaging using  $\text{Bi}_3^+$  ion beam: **(l)** bright field image; **(m, n)** ToF-SIMS images of  $\text{Cl}^-$  **(m)** and  $\text{PO}_3^-$  **(n)** of the single cell, **(o)** merged image of ToF-SIMS images and LSCM image of DAPI (blue), **(p)** merged image of ToF-SIMS images  $\text{Cl}^-$  (red) and  $\text{PO}_3^-$  (green) and LSCM images of EYFP-HMGB1 (blue). The ToF-SIMS images of  $\text{Cl}^-$  and  $\text{PO}_3^-$  were acquired at  $m/z$  35 and 79, respectively.

## **COSIMSi visualizes interaction between HMGB1 and cisplatin damaged DNA**

Before performing COSIMS imaging on HeLa cells treated by cisplatin, we compared the fluorescent labeling strategies of HMGB1 protein, including conventional immunostaining and fluorescent protein fusion (Fig. 2). HeLa cells transfected by pCMV-N-Flag-HMGB1(wt), pEYFP-HMGB1(wt) plasmids, or without plasmid as blank control group, were cultured on an addressable silicon wafer, respectively. Twenty-four hours later, the cells were incubated with fresh culture medium containing 50  $\mu$ M cisplatin for another 24 h. The IC<sub>50</sub> of cisplatin against HeLa cells is 10 – 20  $\mu$ M, which were usually determined with a 48 h or longer incubation of cells with cisplatin<sup>26</sup>. Thus, we could observe that there were still enough viable HeLa cells after incubation with 50  $\mu$ M cisplatin for 24 h (Fig. 2Ia). The cisplatin treated cells were fixed with pre-cold pure ethanol and permeabilized using 0.1% PBST. Then the wild-type HeLa cells and pCMV-N-Flag-HMGB1(wt) transfected HeLa cells were respectively incubated with anti-HMGB1 primary antibody, FITC-labeled secondary antibody and DAPI, and the EYFP-HMGB1 overexpressed HeLa cells were stained by DAPI only. The HeLa cells were washed thoroughly with PBS and ammonium acetate buffer (pH = 7.4) before lyophilized, followed by LSCM and ToF-SIMS imaging successively.

As shown in Fig. 2Ib, IIb, IIIb, the LSCM images of DAPI well rendered the cell nuclei, and HMGB1 protein was found to locate mainly in the nucleus region as indicated by immunofluorescence or EYFP images (Fig. 2Ic, IIc, IIIc). Notably, without cisplatin treatment, HMGB1 was demonstrated to distribute in the whole HeLa cells (Fig. 1d). Meanwhile, the ToF-SIMS images (Fig. 2Id, IIId, IIIId) indicate again that cisplatin mainly located in the nucleus region.

Next, we merged the LSCM images of DAPI and EYFP-fused or immunostained HMGB1 with SIMS images of cisplatin rendered by [PtCN]. The overlaps (navy spots in Fig. 2Ie, IIe, IIIe) of LSCM signals of DAPI and HMGB1 indicate the formation of DNA-HMGB1 complex, those of LSCM signal of HMGB1 and SIMS signal of cisplatin show proximity of HMGB1 and cisplatin (yellow spots in Fig. 2If, IIIf, IIIIf), and those of LSCM signals of DAPI and HMGB1, and SIMS signal of cisplatin evidence the formation of the HMGB1-Pt-DNA ternary complex inside the cells (white spots in Fig. 2Ig, IIg, IIIg). A java program was developed to extract the overlapping region of LSCM signals of DAPI/HMGB1 and SIMS signal of cisplatin. As shown in Fig. 2Ih, IIh, IIIh, the extracted signals significantly increase in intensity in the HMGB1 or EYFP-HMGB1 overexpressed HeLa cells in comparison with those in the wild-type HeLa cells. This indicates that more HMGB1-Pt-DNA complex formed in the HMGB1 or EYFP-HMGB1 overexpressed HeLa cells than in the wild-type ones, being well consistent with previous reports that overexpressed HMGB1 could prevent the cisplatin-damaged DNA from NER, promoting the formation of HMGB1-Pt-DNA complex in cells.<sup>3,10</sup> To our best knowledge, it is the first report for the observation of presence of HMGB1-Pt-DNA complex in single cell level. Because EYFP fusion not only provided high quality fluorescence images for visualization of HMGB1, but also simplified the experiments due to omission of immunostaining, we used EYFP fusion to label HMGB1 for rest of our experiments.

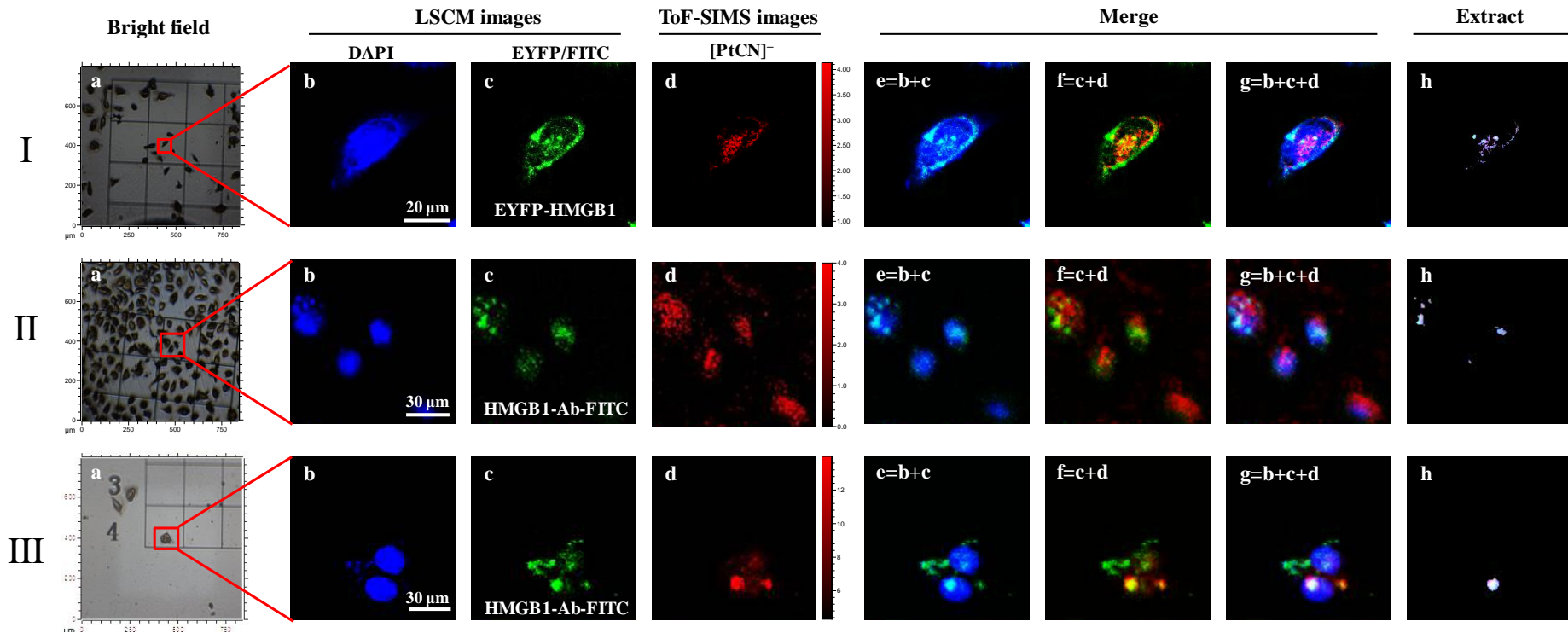


**Fig. 2 | COSIMS imaging of different types of HeLa cells treated with 50  $\mu$ M cisplatin. (I)** HeLa cells transfected by pEYFP-HMGB1(wt) plasmid; **(II)** wild type HeLa cells; **(III)** HeLa cells transfected by pCMV-N-Flag-HMGB1(wt) plasmid; **(a)** bright field images; **(b)** fluorescence images of DAPI ( $\lambda_{\text{ex}} = 405 \text{ nm}$ ;  $\lambda_{\text{em}} = 425 - 475 \text{ nm}$ ); **(Ic)** fluorescence images of EYFP-HMGB1 ( $\lambda_{\text{ex}} = 488 \text{ nm}$ ;  $\lambda_{\text{em}} = 500 - 600 \text{ nm}$ ); **(IIc, IIIc)** immunofluorescence images of HMGB1 ( $\lambda_{\text{ex}} = 488 \text{ nm}$ ;  $\lambda_{\text{em}} = 500 - 600 \text{ nm}$ ); **(d)** ToF-SIMS image of  $[\text{PtCN}]^-$  acquired at  $m/z$  220, 221 and 222; **(e)** merged fluorescent images of DAPI (blue) and HMGB1 FITC-conjugated secondary antibody (green, **IIc, IIIc**) or EYFP-fused (green, **Ic**); **(f)** merged images of HMGB1 FITC-conjugated secondary antibody (**IIc, IIIc**) or EYFP-fused (**Ic**) and SIMS image of  $[\text{PtCN}]^-$  (red); **(g)** merged images of fluorescence images of DAPI, HMGB1 and SIMS image of  $[\text{PtCN}]^-$ ; **(h)** extracted images from **(g)** for better contrast.

## Dose-dependent and time-dependent COSIMS imaging

To verify whether the white spots in the merged and the extracted signals indeed represent the formation of HMGB1-Pt-DNA complex, experiments with different concentrations of cisplatin and incubation time were carried out. As shown in Fig. 3, when the concentration of cisplatin increased, the signal of  $[\text{PtCN}]^-$  in the ToF-SIMS images (Fig. 3Id, IIId, IIIId) became stronger. Moreover, the overlapped spots in the merged images of DAPI, HMGB1 and  $[\text{PtCN}]^-$  (Fig. 3Ig, IIg, IIIg) became denser, larger and brighter, so did the extracted signals (Fig. 3Ih, IIh, IIIh). These results verified the fact that higher level of cisplatin induced more Pt damage on DNA and as a consequence more HMGB1 assembly at the lesion sites. Meanwhile, upon the increased concentration of cisplatin, the viability of HeLa cells significantly decreased as shown in the Fig. 3Ia, IIa, IIIa. Interestingly, the fluorescence images of EYFP-HMGB1 and DNA, and the ToF-SIMS images of cisplatin all depicted the formation of apoptotic bodies inside HeLa cells treated with 50 and 100  $\mu\text{M}$  cisplatin for 24 h (Fig. 3II, 3III). To balance the viability of the cells and the observation of overlapped spots, 50  $\mu\text{M}$  cisplatin was used in the following experiments.

An uptake kinetics study with a gradient of 3 h, 6 h, 12 h and 24 h incubation after 50  $\mu\text{M}$  cisplatin was added to the culture medium was carried out. As depicted in Fig. 4, little overlapped signals of fluorescence images of DAPI/EYFP-HMGB1 and SIMS images of cisplatin could be observed in the merged images recorded on the HeLa cells incubated with cisplatin for 3 or 6 hours (Fig. 4Ie – h, 4IIe – h), which agree with the well accepted fact that 3 h and 6 h is not long enough for cisplatin entering the cell nucleus to bind to DNA<sup>4</sup>. When the incubation time was increased to 12 h, tiny and weak overlapped signals were observed in the merged images of LSCM images of DAPI/EYFP-HMGB1 and the SIMS image of cisplatin in the nuclear areas (Fig. 4IIIe – h). Moreover, the viable cells on the silicon wafer significantly decreased with increase in the incubation time (Fig. 4Ia, IIa, IIIa). When the incubation time was further extended to 24 h, the overlapped signals in the merged images of LSCM images and SIMS images substantially increased in intensity (Fig. 4IVe – h), indicating that more HMGB1-Pt-DNA ternary complex formed in the nuclei. In addition, the density of the survival cells further reduced to an ideal level for our COSIMS imaging (Fig. 4IVa).

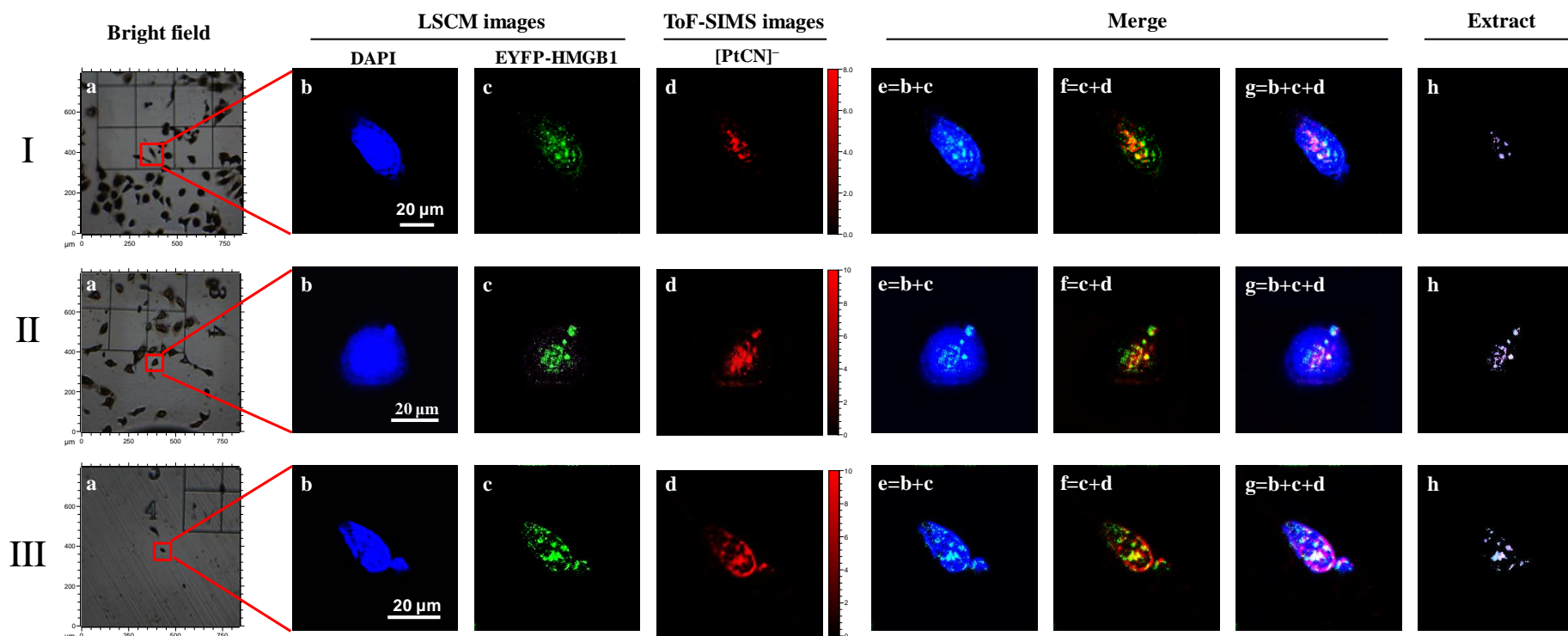


**Fig. 3 | COSIMS imaging of HeLa cells transfected by pEYFP-HMGB1(wt) plasmid and treated with different concentration of cisplatin. (I) 25 μM; (II) 50 μM; (III) 100 μM. (a)** Bright field images; **(b)** fluorescence images of DAPI ( $\lambda_{\text{ex}} = 405 \text{ nm}$ ;  $\lambda_{\text{em}} = 425 - 475 \text{ nm}$ ); **(c)** fluorescence images of EYFP-HMGB1 ( $\lambda_{\text{ex}} = 488 \text{ nm}$ ;  $\lambda_{\text{em}} = 500 - 600 \text{ nm}$ ); **(d)** ToF-SIMS images of  $[\text{PtCN}]^-$  acquired at  $m/z$  220, 221 and 222; **(e)** merged fluorescent images of DAPI (blue) and EYFP-HMGB1 (green); **(f)** merged images of EYFP-HMGB1 (green) and SIMS image of  $[\text{PtCN}]^-$  (red); **(g)** merged images of fluorescence images of DAPI, HMGB1 and SIMS image of  $[\text{PtCN}]^-$ ; **(h)** extracted images from (g) for better contrast.

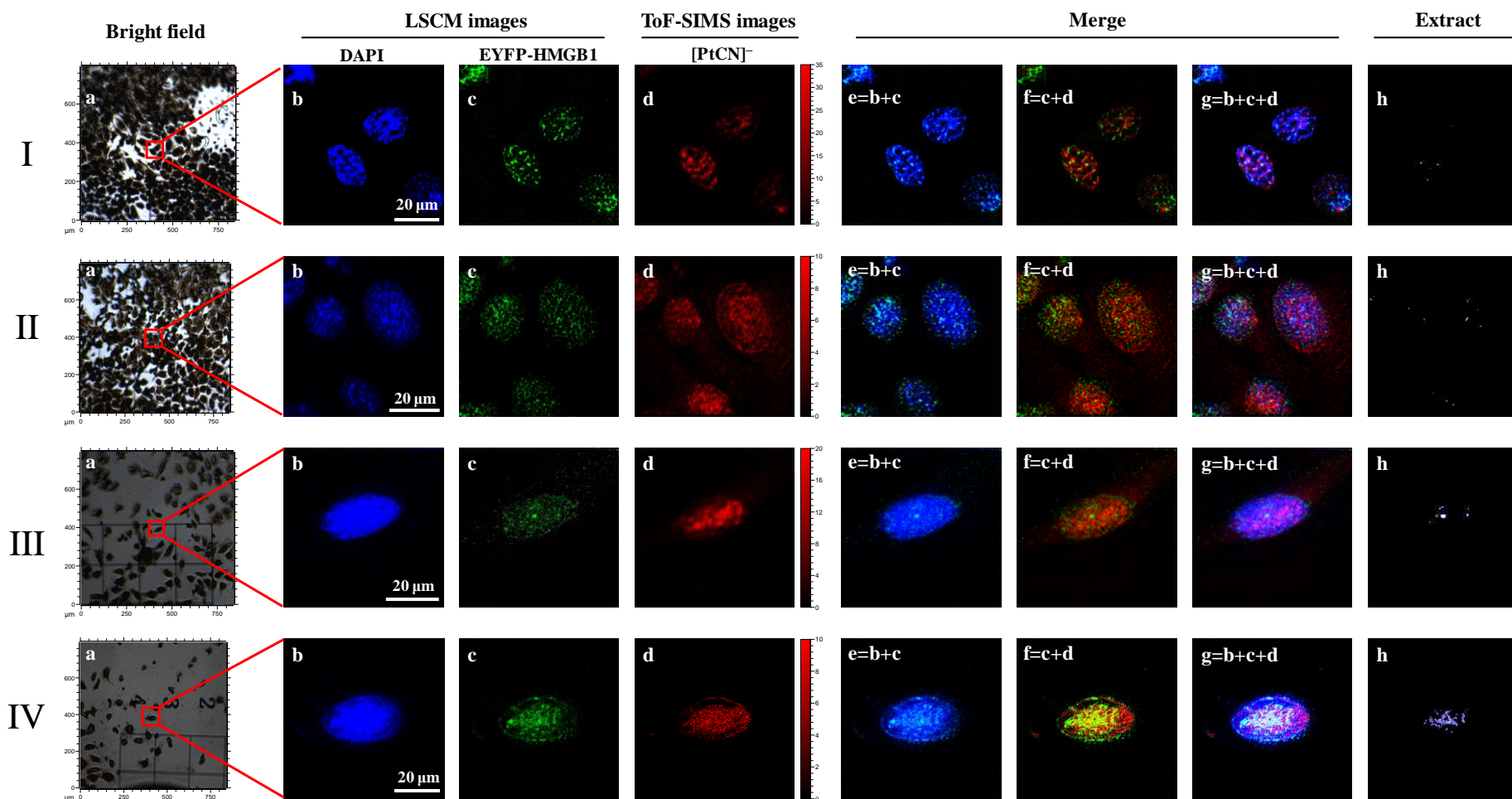


**Fig. 4 | COSIMS imaging of HeLa cells transfected by pEYFP-HMGB1(wt) plasmid treated with 50  $\mu$ M cisplatin for different time. (I) 3 h; (II) 6 h; (III) 12 h; (IV) 24 h. (a) Bright field images; (b) fluorescence images of DAPI ( $\lambda_{\text{ex}} = 405 \text{ nm}$ ;  $\lambda_{\text{em}} = 425 - 475 \text{ nm}$ ); (c) fluorescence**

images of EYFP-HMGB1 ( $\lambda_{\text{ex}} = 488 \text{ nm}$ ;  $\lambda_{\text{em}} = 500 - 600 \text{ nm}$ ); **(d)** ToF-SIMS images of  $[\text{PtCN}]^-$  acquired at  $m/z$  220, 221 and 222; **(e)** merged fluorescent images of DAPI (blue) and EYFP-HMGB1 (green); **(f)** merged images of EYFP-HMGB1 (green) and SIMS image of  $[\text{PtCN}]^-$  (red); **(g)** merged images of fluorescence images of DAPI, HMGB1 and SIMS image of  $[\text{PtCN}]^-$ ; **(h)** extracted images from **(g)** for better contrast.

## **Negative control COSIMS imaging by site-specific mutation of HMGB1 and other DNA binding proteins**

More control experiments were performed to verify further our COSIMS imaging method (Fig. 5). Since the Phe37 residue on HMGB1 is crucial for the recognition of HMGB1 to cisplatin damaged DNA<sup>9</sup>, we did a site-specific mutation at Phe37 (F37A) of HMGB1 (Supplementary Fig. 6). The mutant protein was also fused with EYFP for LSCM imaging. With the F37A mutant, the binding of the protein to the Pt damaged DNA is assumed to significantly weakened. Indeed, our COSIMS imaging showed that unlike the wild type EYFP-HMGB1, the EYFP-HMGB1(F37A) mutated protein appeared to distribute homogeneously inside the cell instead of enriching in the nucleic area (Fig. 5Ic). Moreover, the fluorescence signals of EYFP-HMGB1(F37A) did not overlap with the SIMS signal of [PtCN]<sup>-</sup> (Fig. 5If – h), being consistent with the fact that HMGB1(F37A) could not recognize the cisplatin damaged DNA.

To exclude the unspecific binding or coincident overlap of fluorescence and SIMS images, a DNA binding protein, Smad3, was also employed as control to verify our COSIMS imaging method further. Herein, Smad3 was fused with enhanced green fluorescent protein (EGFP) and imaged by LCSM in a similar way as described above (Fig. 5II). From the merged images shown in Fig. 5IIe, Smad3 mainly located in nuclear area rendered by DAPI, indicating that they bound to nuclear DNA. However, Smad3 did not co-localize with cisplatin indicated by [PtCN]<sup>-</sup> (Fig. 5IIf – h), simply because they cannot recognize or interact with Pt damaged DNA, in consistence with previous reports<sup>4,10</sup>. Interestingly, within the nuclear region, the spots with stronger signal of [PtCN]<sup>-</sup> always corresponded to weaker signal of EGFP-Smad3 (Fig. 5IIg, g). This result implies that cisplatin damage on DNA appears to block the binding of Smad3 to DNA.

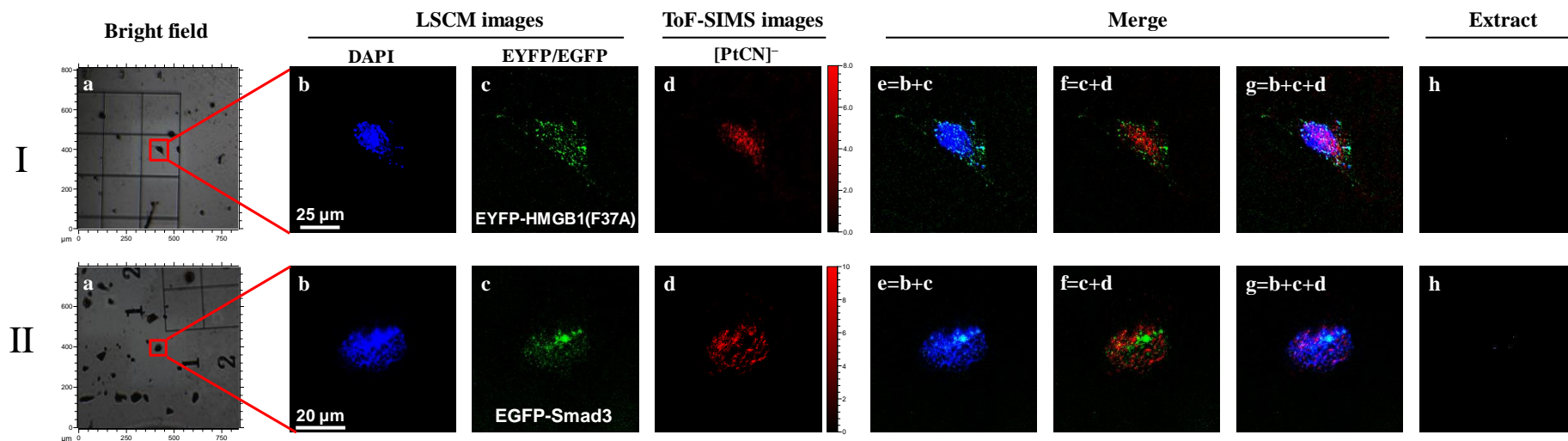


**Fig. 5 | COSIMS imaging of different types of HeLa cells treated with 50  $\mu$ M cisplatin. (I)** HeLa cells transfected by EYFP-HMGB1(F37A) plasmid; **(II)** HeLa cells transfected by EGFP-Smad3 plasmid. **(a)** Bright field images; **(b)** fluorescence images of DAPI ( $\lambda_{\text{ex}} = 405$  nm;  $\lambda_{\text{em}} = 425 - 475$  nm); **(Ic)** fluorescence images of EYFP-HMGB1 ( $\lambda_{\text{ex}} = 488$  nm;  $\lambda_{\text{em}} = 500 - 600$  nm); **(IIc)** fluorescence images of EGFP-Smad3 ( $\lambda_{\text{ex}} = 488$  nm;  $\lambda_{\text{em}} = 500 - 600$  nm); **(d)** ToF-SIMS image of  $[\text{PtCN}]^-$  acquired at  $m/z$  220, 221 and 222; **(e)** merged fluorescent images of DAPI (blue) and EYFP-HMGB1(F37A) (green, **Ic**), EGFP-Smad3 (green, **IIc**); **(f)** merged images of EYFP-HMGB1(F37A) (green, **Ic**), EGFP-Smad3 (green, **IIc**) and SIMS image of  $[\text{PtCN}]^-$  (red); **(g)** merged images of fluorescence images of DAPI/EYFP-HMGB1(F37A) (**Ic**), EGFP-Smad3 (**IIc**), and SIMS image of  $[\text{PtCN}]^-$ ; **(h)** extracted images from **(g)** for better contrast.

## Discussion

In this work, we directly observed for the first time the recognition and interaction of HMGB1 towards cisplatin damaged DNA inside cells. Previous research strategies for the interaction of proteins with DNA are mostly based on electrophoresis. Classical tools to investigate the protein-DNA complexes include Comet assay, DNA footprinting and electrophoretic mobility shift assay (EMSA), *etc.* Other strategies such as methylation interference and chromatin immunoprecipitation *etc.* provide near base-pair resolution insights for the protein-DNA interactions and the functional organization of the genome<sup>27</sup>. However, these methods were generally applied for genome DNA and the proteins extracted from cells in cell-free media. *In vivo* footprinting assay can assess proteins specific binding sites throughout the genome inside the cells. Fluorescence *in situ* hybridization (FISH) is usually used to localize a specific DNA sequences on chromosomes, but not a specific drug damaged site of DNA. Classical imaging methods, for example, immunofluorescent microscopy is difficult to locate a specific nonfluorescent DNA damage, neither could traditional laser confocal imaging *in situ* observe the interaction of non-fluorescent drugs and their target DNA. To our best knowledge, the COSIMSi protocol developed in this work is the first one for *in situ* studying the interaction of proteins with drug damaged DNA at single cell level. The binding of HMGB1 to cisplatin damaged DNA were successfully observed in cell nucleus region. The results demonstrate that our method is a universal tool to visualize the interaction between a non-fluorescent drug damaged DNA and a protein of interest inside cells.

During the past decade, a number of correlated optical and SIMS microscopy imaging methods have been developed to explore the procedure of benthic marine nitrogen fixation<sup>21</sup>, protein turnover in cells<sup>16,18-20,28</sup>, stem cell division and metabolism<sup>17</sup>, as well as the subcellular distribution/release of metal based anticancer complexes<sup>16,23,25,29</sup>. Due to its high lateral resolution (50 – 100 nm) and mass resolution (> 10,000), NanoSIMS was mostly used in these studies above except for our work which applied ToF-SIMS in combination with fluorescence confocal microscopy imaging to map the subcellular distribution of a house-made organometallic ruthenium anticancer complex<sup>25</sup>. In order to perform NanoSIMS imaging, cells were generally embedded with resin and sliced into ultrathin films<sup>18,20,23</sup>, which request high temperature treatment (65 °C), probably disturbing the finely controlled cell structure. Compared to NanoSIMS, ToF-SIMS can simultaneously detect all ions over a much wider *m/z* range, and generate molecule ions or large fragment ions so as to provide more structural information to chemicals of interest.<sup>30</sup> More importantly, we have recently demonstrated that ToF-SIMS imaging could achieve a 230 – 290 nm lateral resolution when it was used to map directly the distribution of drug candidates in lyophilized cells without needing to section cells<sup>25</sup>. Furthermore, the lateral resolution of ToF-SIMS and LSCM right match each other,<sup>25</sup> making it unnecessary to sharpen the images gained by a lower resolution imaging technique to merge with the ones obtained by a higher resolution imaging approach<sup>31-33</sup>.

For the visualization of HMGB1 by LSCM in single cells, immunofluorescence imaging of proteins using antibodies is a classic strategy. This method, however, requested complicated cell treatment, e.g. cell permeation and rigorous washing, which often leads to detachment of cells on silicon wafer. Recently, the bio-orthogonal technique combined click reaction has been successfully utilized to insert bifunctional labels, i.e. fluorescence and mass labels, to the proteins of interest for mapping their subcellular distribution by optical and NanoSIMS imaging<sup>18,19</sup>. Genetically encoded fluorescent proteins have also been widely used as fused indicators to trace intracellular locations of targeted proteins and to monitor the dynamic signaling and/or dimerization of proteins of interest<sup>34</sup>. In this work, we genetically encoded the enhanced yellow fluorescent protein (EYFP) into the HMGB1 as indicators for visualizing the recognition and interaction between the protein and cisplatin damaged DNA. This strategy allowed an rapid and efficient location of HMGB1 in single cells, and the coupling EYFP with HMGB1 did not hinder the interaction between the protein and Pt damaged DNA.

Another advantage of our COSIMSi strategy is the use of addressable silicon wafer for cell culture, which allows us to locate easily one or a few single cells for sequential optical and mass spectrometric imaging, and assists the exact alignment of optical images and SIMS images for the same single cells. The last but not least, ToF-SIMS is affordable for more research institutes, and our COSIMSi method can be more widely applied for exploring the interactions of drugs with their biological targets at single cell level.

The Smad family proteins, i.e. Smad3 is a DNA binding protein, and also important signal transducers for receptors of the transforming growth factor beta (TGF- $\beta$ ) superfamily. They play a crucial role in regulating cell development and growth. Smad3 belongs to receptor-regulated Smads (R-Smads) subfamily, and acts as transcription factors that participate in regulating the gene expression<sup>35</sup>. Our studies herein demonstrated that cisplatin damage on DNA blocked the binding of the Smad family transcription factors with genes. This implies that cisplatin damage on DNA may impact the transcriptional function of Smad3 by disrupting the interactions of the proteins with DNA, which may contribute to the anticancer efficiency of cisplatin. More importantly, these results further verify the specificity and reliability of the developed COSIMSi method for *in situ* visualizing the recognition and interactions between proteins and drug damaged DNA inside cells.

## Conclusion

Taking the advantages of LSCM imaging for localization of specific proteins and ToF-SIMS imaging for visualization of platinum-based drugs at single cell level, we have developed a correlated optical and mass spectrometric microscopy imaging approach for *in situ* visualization of recognition and interaction of non-specific DNA-binding protein HMGB1 with cisplatin damaged DNA inside cells. The correlation of SIMS and LSCM imaging combines the advantages of the two techniques. The overlap of fluorescence signals of DNA/HMGB1 and ToF-SIMS signals of cisplatin increased in

intensity in a dose-/time-dependent manner, suggesting the formation of HMGB1-Pt-DNA ternary complex in nuclei. Moreover, the application of the developed COSIMSi method revealed for the first time that cisplatin damage on DNA prevents transcription regulator Smad3 from binding to DNA, perhaps accounting for inhibition on the transcription and replication of DNA. We anticipate further application of this unique combined imaging approach for investigating interactions of damaged DNA with other DNA-binding proteins.

## Online content

Any methods, additional references, Nature Research reporting summaries, source data, extended data, supplementary information, acknowledgements, peer review information; details of author contributions and competing interests; and statements of data and code availability are available at <https://doi.org...>

## References

- 1 Casini, A. & Reedijk, J. Interactions of anticancer Pt compounds with proteins: an overlooked topic in medicinal inorganic chemistry? *Chem. Sci.* **3**, 3135-3144 (2012).
- 2 Shu, X., Xiong, X., Song, J., He, C. & Yi, C. Base - Resolution Analysis of Cisplatin - DNA Adducts at the Genome Scale. *Angew. Chem. Int. Ed.* **55**, 14246-14249 (2016).
- 3 Jung, Y. & Lippard, S. J. Direct Cellular Responses to Platinum-Induced DNA Damage. *Chem. Rev.* **107**, 1387-1407 (2007).
- 4 Jamieson, E. R. & Lippard, S. J. Structure, Recognition, and Processing of Cisplatin-DNA Adducts. *Chem. Rev.* **99**, 2467-2498 (1999).
- 5 Zeng, W. *et al.* Proteomic Strategy for Identification of Proteins Responding to Cisplatin-Damaged DNA. *Anal. Chem.* **91**, 6035-6042 (2019).
- 6 Furuta, T. *et al.* Transcription-coupled Nucleotide Excision Repair as a Determinant of Cisplatin Sensitivity of Human Cells. *Cancer Res.* **62**, 4899-4902 (2002).
- 7 Kunkel, T. A. & Erie, D. A. DNA mismatch repair. *Annu. Rev. Biochem.* **74**, 681-710 (2005).
- 8 Baxevanis, A. D. & Landsman, D. The HMG-1 box protein family: classification and functional relationships. *Nucleic Acids Res.* **23**, 1604-1613 (1995).
- 9 Ohndorf, U.-M., Rould, M. A., He, Q., Pabo, C. O. & Lippard, S. J. Basis for recognition of cisplatin-modified DNA by high-mobility-group proteins. *Nature* **399**, 708 (1999).
- 10 Wang, D. & Lippard, S. J. Cellular processing of platinum anticancer drugs. *Nat. Rev. Drug Discov.* **4**, 307 (2005).
- 11 Passarelli, M. K. *et al.* The 3D OrbiSIMS-label-free metabolic imaging with subcellular lateral resolution and high mass-resolving power. *Nat. Methods* **14**, 1175-1183 (2017).
- 12 Zenobi, R. Single-Cell Metabolomics: Analytical and Biological Perspectives. *Science* **342**, 1201-1211 (2013).
- 13 Bodzon-Kulakowska, A. & Suder, P. Imaging Mass Spectrometry: Instrumentation, Applications, and Combination with Other Visualization Techniques. *Mass Spectrom. Rev.* **35**, 147-169 (2016).
- 14 Neumann, E. K., Do, T. D., Comi, T. J. & Sweedler, J. V. Exploring the Fundamental Structures

- of Life: Non-Targeted, Chemical Analysis of Single Cells and Subcellular Structures. *Angew. Chem. Int. Ed.* **58**, 9348-9364 (2019).
- 15 Han, J. *et al.* Imaging of protein distribution in tissues using mass spectrometry: An interdisciplinary challenge. *TrAC, Trends Anal. Chem.* **112**, 13-28 (2019).
- 16 Zhang, D.-S. *et al.* Multi-isotope imaging mass spectrometry reveals slow protein turnover in hair-cell stereocilia. *Nature* **481**, 520-524 (2012).
- 17 Steinhäuser, M. L. *et al.* Multi-isotope imaging mass spectrometry quantifies stem cell division and metabolism. *Nature* **481**, 516-519 (2012).
- 18 Vreja, I. C. *et al.* Secondary-Ion Mass Spectrometry of Genetically Encoded Targets. *Angew. Chem. Int. Ed.* **54**, 5784-5788 (2015).
- 19 Kabatas, S. *et al.* Boron-Containing Probes for Non-optical High-Resolution Imaging of Biological Samples. *Angew. Chem. Int. Ed.* **58**, 3438-3443 (2019).
- 20 Saka, S. K. *et al.* Correlated optical and isotopic nanoscopy. *Nat. Commun.* **5**, 3664-3671 (2014).
- 21 Dekas, A. E., Poretsky, R. S. & Orphan, V. J. Deep-Sea Archaea Fix and Share Nitrogen in Methane-Consuming Microbial Consortia. *Science* **326**, 422-426 (2009).
- 22 Lechene, C. P., Luyten, Y., McMahon, G. & Distel, D. L. Quantitative imaging of nitrogen fixation by individual bacteria within animal cells. *Science* **317**, 1563-1566 (2007).
- 23 Legin, A. A. *et al.* NanoSIMS combined with fluorescence microscopy as a tool for subcellular imaging of isotopically labeled platinum-based anticancer drugs. *Chem. Sci.* **5**, 3135 (2014).
- 24 Zhang, Y. *et al.* Luminescent cyclometallated platinum(II) complexes: highly promising EGFR/DNA probes and dual-targeting anticancer agents. *Inorg. Chem. Front.* **5**, 413-424 (2018).
- 25 Liu, S. Y. *et al.* Correlated mass spectrometry and confocal microscopy imaging verifies the dual-targeting action of an organoruthenium anticancer complex. *Chem. Commun.* **53**, 4136-4139 (2017).
- 26 Sandman, K. E. & Lippard, S. J. in *Cisplatin: Chemistry and Biochemistry of a Leading Anticancer Drug* (ed Bernhard Lippert) 523-536 (Verlag Helvetica Chimica Acta, 1999).
- 27 Venters, B. J. Insights from resolving protein-DNA interactions at near base-pair resolution. *Brief. Funct. Genomics* **17**, 80-88 (2018).
- 28 Senyo, S. E. *et al.* Mammalian heart renewal by pre-existing cardiomyocytes. *Nature* **493**, 433-436 (2013).
- 29 Proetto, M. T. *et al.* Cellular Delivery of Nanoparticles Revealed with Combined Optical and Isotopic Nanoscopy. *ACS Nano* **10**, 4046-4054 (2016).
- 30 Ostrowski, S. G., Van Bell, C. T., Winograd, N. & Ewing, A. G. Mass spectrometric imaging of highly curved membranes during *Tetrahymena* mating. *Science* **305**, 71-73 (2004).
- 31 Van de Plas, R., Yang, J. H., Spraggins, J. & Caprioli, R. M. Image fusion of mass spectrometry and microscopy: a multimodality paradigm for molecular tissue mapping. *Nat. Methods* **12**, 366-U138 (2015).
- 32 Vollnhals, F. *et al.* Correlative Microscopy Combining Secondary Ion Mass Spectrometry and Electron Microscopy: Comparison of Intensity-Hue-Saturation and Laplacian Pyramid Methods for Image Fusion. *Anal. Chem.* **89**, 10702-10710 (2017).
- 33 de Boer, P., Hoogenboom, J. P. & Giepmans, B. N. G. Correlated light and electron microscopy: ultrastructure lights up! *Nat. Methods* **12**, 503-513 (2015).
- 34 Giepmans, B. N. G., Adams, S. R., Ellisman, M. H. & Tsien, R. Y. The fluorescent toolbox for assessing protein location and function. *Science* **312**, 217-224 (2006).

- 35 Derynck, R. & Zhang, Y. E. Smad-dependent and Smad-independent pathways in TGF- $\beta$  family signalling. *Nature* **425**, 577-584 (2003).
- 36 Li, N. *et al.* Single-Molecule Imaging Reveals the Activation Dynamics of Intracellular Protein Smad3 on Cell Membrane. *Sci. Rep.* **6**, 33469 (2016).

## Acknowledgements

We thank Prof. Andrew Ewing at the Department of Chemistry and Molecular Biology, University of Gothenburg, Sweden, for stimulating discussion and helpful comments. We thank the NSFC (grant nos. 21575145, 91543101, 21505141, 21605146, 21635008, 21621062, 21790390 and 21790392) for support. Y.Z. thank the Youth Innovation Promotion Association of Chinese Academy of Sciences (grant no. 2017051), and Q.L. thank the Beijing Municipal Natural Science Foundation (grant no.7182190) for support.

## Author contributions

F.W. and Y.Zhao conceived and designed the project. F.W. supervised the project. Y.L., K.W., F.J., Q.L. and L.C. performed the LSCM experiments, K.W., F.J., Z.W., Y.Zhang and S.L. performed the ToF-SIMS experiments. Y.L., L.C. and L.Q. performed the construction of EYFP-HMGB1 and western blot experiments. N.L. constructed EGFP-Smad3 plasmid under supervision of X.F. P.D. and F.G. edited the Java program. Y.L., K.W., F.J., F.W. and Y.Zhao analyzed data. Y.L., K.W., F.J., L.C., Y.Zhao and F.W. wrote and revised the manuscript.

## Competing interests

The authors declare no competing interests.

## Additional information

**Supplementary information** is available for this paper.

**Correspondence and requests for materials** should be addressed to F.W. or Y.Zhao.

## Methods

### Materials and Reagents

The human cervical cancer cell line HeLa was obtained from the Center for Cell Resource of Peking Union Medical College Hospital (Beijing, China), and maintained in DMEM (Invitrogen, USA) supplemented with 10% fetal bovine serum (FBS, Invitrogen, USA) and 1% penicillin–streptomycin (PS, Invitrogen, USA). Non-specific DNA fluorescent probe DAPI was purchased from Invitrogen (USA), anti-HMGB1 primary antibody, anti-actin primary antibody from Abcam Ltd (Cambridge, UK), and secondary antibody from Zhongshanjinqiao Ltd (Beijing, China). Nitrocellulose membrane was purchased from Millipore, fast Site-Directed Mutagenesis Kit from TianGen biotech. FuGENE® HD Transfection Reagent was purchased from Promega Corporation (Madison, WI, USA), pEYFP-C1 from Clontech, HisTrap FF crude from GE Healthcare (Chicago, IL, USA). The addressable silicon wafers with 200×200 μm square matrices was house-made following the protocol described in our previous report<sup>25</sup>.

### Plasmids construction

The codon optimized HMGB1 gene sequence obtained from Origene Ltd (Beijing, China) was amplified by PCR and then cloned to pCMV-N-Flag and pEYFP-N1 vector, to get the pCMV-N-Flag-HMGB1(wt) and pEYFP-HMGB1(wt) plasmids, respectively. The corresponding HMGB1(F37A) site mutant plasmids was constructed by 18 cycles PCR with the primers, 5'-CACCCAGATGCTTCAGTCAACTTCTCAGAGGCTTCTAAGAAGTGCTCAGAGAGGTGGAAG-3' (F37A-F) and 5'-CTTCCACCTCTCTGAGCACTTCTTAGAAGCCTCTGAGAAGTTGACTGAAGCATCTGGGTG-3' (F37A-R), to get the pEYFP-HMGB1(F37A) plasmids. The EGFP-Smad3 plasmid was constructed as previously described<sup>36</sup>.

### Cell Culture, staining and sample preparation

For correlated LSCM and ToF-SIMS imaging, HeLa cancer cells were seeded on an house-made addressable silicon wafer at a density of 1×10<sup>4</sup> cells/cm<sup>2</sup> in a cell culture dish with DMEM medium and incubated at 310 K under a humidified atmosphere containing 5% CO<sub>2</sub> to incubate overnight for cell attachment. The cells were then transfected with 1 μg each plasmid described above by FuGENE® HD (Promega, Madison, WI, USA) following the manufacture instructions. After 24 h of transfection, 1 mM cisplatin stock solution was diluted with culture medium to requested concentrations and added into respective culture dish, then HeLa cells were incubated with cisplatin for 24 h unless otherwise stated. Cell samples for control were treated under the same conditions except the addition of drug and/or plasmid transfection. The cells were fixed with pure ethanol pre-cooled in a 253 K freezer for 20 min, and permeabilized using 0.1% PBST (1 mL PBS + 1 uL Tween 20) for 15 minutes at 277 K. Then the wild type and pCMV-N-Flag-HMGB1(wt) transfected HeLa cells were

incubated with 1 mL horse serum for 1 h at 277 K followed by PBST washing 3 times (10 mins each time), and then the cells were incubated with 1 mL diluted anti-HMGB1 primary antibody (mouse anti-human HMGB1 monoclonal antibody, 1:10000 dilution, Abcam, ab77302) for 1 h in room temperature. After washed by PBST 3 times (10 min each time) in horizontal shaker, the FITC-labeled secondary antibody (goat anti-mouse antibody, 1:500 dilution) was added to the cell culture disk and incubated for 40 mins at room temperature. Next, after removing the excess of secondary antibody and adding PBS for washing 3 times (10 mins for each time), the fluorescence dye DAPI ( $5 \mu\text{g mL}^{-1}$ ) in PBS was added for 10 min incubation to stain nuclear DNA. The EYFP-HMGB1 overexpressed HeLa cells were not added the primary antibody and the secondary antibody, but stained by DAPI only. After that, the sample was thoroughly washed three times with PBS followed by three times washing with ammonium acetate (150 mM, pH = 7.4), then immersed into liquid  $\text{N}_2$  for quick freezing, and transferred intermediately into a lyophilizer (LGJ-12, Beijing Songyuanhuaxing Technology Develop Co., Ltd) at 193 K to 208 K for freeze-drying overnight.

### **Laser scanning confocal microscopy (LSCM)**

The fluorescence imaging was performed on FV1000-IX81 confocal laser scanning microscopy through an IX81 inverted microscope with the 100 $\times$  oil-immersion lens and 40 $\times$  objective lens (Olympus, Tokyo, Japan). For nucleus dye DAPI, the excitation wavelength was 405 nm and emission wavelength 425 – 475 nm. For HMGB1 Ab-FITC,  $\lambda_{\text{ex}} = 488 \text{ nm}$ ,  $\lambda_{\text{em}} = 500 - 600 \text{ nm}$ . For EYFP-HMGB1 fusion,  $\lambda_{\text{ex}} = 488 \text{ nm}$ ,  $\lambda_{\text{em}} = 500 - 600 \text{ nm}$ . For EGFP fused proteins,  $\lambda_{\text{ex}} = 488 \text{ nm}$ ,  $\lambda_{\text{em}} = 500 - 600 \text{ nm}$ . The images were collected and analyzed using the OLYMPUS FLUOVIEW software version 3.1.

### **ToF-SIMS**

ToF-SIMS imaging was carried out with a ToF-SIMS 5 instrument (ION-ToF GmbH, Münster, Germany) equipped with a 30 keV liquid metal primary ion source. The high-lateral-resolution (*ca.* 200 – 300 nm) images of single cell were recorded using  $\text{Bi}_3^+$  primary ion gun with an electron flood gun for charge neutralization. Imaging signal was collected with 256 $\times$ 256 pixels in negative mode after sputtering 5 – 15 cycles with 10 keV Ar-cluster ion beam to remove the cell membrane and other impurities on the cell surface. The sputter view was larger than the analytical scan view of which the size was the same as that of confocal imaging. Due to the difference among individual cell samples, the scan times of each sample varied from 1000 to 3000 to obtain high quality images. The mass images were collected and plotted with the Surface Lab software (version 6.4 ION-ToF GmbH). The mass were calibrated using the signals of  $\text{C}^-$ ,  $\text{CH}^-$ ,  $\text{CH}_2^-$ ,  $\text{C}_2^-$ ,  $\text{C}_2\text{H}^-$ . Region of interest were created for desired cells. The image of cisplatin was constructed by sum of signals of  $[\text{}^{194}\text{PtCN}]^-$ ,  $[\text{}^{195}\text{PtCN}]^-$  and  $[\text{}^{196}\text{PtCN}]^-$  ions and the image of  $[\text{PO}_3]^-$  was used to profile the shape of cells. Shift correction was applied by the software for all the images.

### **Image merging**

The images obtained from LSCM and ToF-SIMS imaging were aligned and merged by Image J (version 1.51j8, NIH, USA). The pixel of the fluorescence images was adjusted to 256×256 pixels. The image of PO<sub>3</sub><sup>-</sup> acquired by ToF-SIMS was mirror transformed and accurately aligned to match the cell position and orientation mapped by LSCM. The images of [PtCN]<sup>-</sup> ions were then processed exactly as those for PO<sub>3</sub><sup>-</sup> images. Once these images were processed separately, they could be merged in different color channels.

### **Image extraction**

To extract the merged signals of fluorescence images of proteins/DNA and SIMS images of cisplatin in the merged images, we developed a program to process the data further. Using Java language, we defined three sets of data from different images as (R, G, B) pixel channel values. The extracted pixels will display only if the corresponding (R, G, B) values are greater than a defined threshold. Otherwise, the pixels' values will be set to zero and leave the position black. By optimizing the threshold, we received satisfied extraction of the overlapped area in the merged images when the threshold was set to 50. The java code is provided in the supporting information.

### **Western blotting**

HeLa cancer cells transfected by pCMV-N-Flag-HMGB1(wt), pEYFP-HMGB1(wt), and pEYFP-HMGB1(F37A) plasmids, respectively, were cultured in a cell culture dishes following the same procedure as described in cell culture subsection. The cells were then harvested by centrifugation at 800 g for 5 min, and the cell pellets were re-suspended in RIPA lysis buffer (Thermo Scientific™, Cat No. 89900, USA) for protein extraction. Each protein extract was dissolved in a loading buffer (pH 6.8) containing 0.5 M Tris-HCl, 20% glycerol, 2% sodium dodecyl sulphate (SDS), bromophenol blue and 10 mM dithiothreitol. The protein samples were loaded and separated by 12% SDS-polyacrylamide gels, then transferred to nitrocellulose (NC) membranes. The NC membranes were blocked with a solution of 5% (w/v) skimmed milk powder in PBST (0.1% (w/v) Tween 20 in PBS (pH 7.5)) for 0.5 h at room temperature, and then incubated with mouse anti-human HMGB1 monoclonal antibody (10000× dilution) or mouse anti-human β-actin monoclonal antibody (10000× dilution), respectively, for 1.5 h at room temperature or overnight at 277 K. Next, the membrane was washed by PBST three times (10 min each time) and incubated with the goat anti mouse HRP-conjugated secondary antibody (1:500 dilution) for 40 min in room temperature. After washed by PBST three times (10 min each time), HRP substrates (Pierce™ ECL, Cat No. 32109) was added to the NC membrane before immediately detected by Tanon 5200 Multi imaging system (Tanon Science & Technology Co., Ltd., Shanghai, China). The intensities of the bands were quantitated using Tanon Gel Imaging System 1D analyzing software (version 4.2).